Power sources coordination through multivariable LPV/Hinf control with application to multi-source electric vehicles

Waleed Nwesaty, Antoneta Iuliana Bratcu, Olivier Sename

Power sources coordination through multivariable LPV/H_∞ control with application to multi-source electric vehicles

Waleed Nwesaty, Antoneta Iuliana Bratcu, Olivier Sename

August 1, 2016

Abstract

In this paper the problem of multi-source power sharing strategy within electric vehicles is considered. Three different kinds of power sources – fuel cell, battery and supercapacitor – compose the power supply system, where all sources are current-controlled and paralleled together with their associated DC-DC converters on a common DC-link. The DC-link voltage must be regulated regardless of load variations corresponding to the driving cycle. The proposed strategy is a robust control solution using a MIMO LPV/H_∞ controller which provides the three current references with respect to source frequency characteristics. The selection of the weighting functions is guided by a genetic algorithm whose optimization criterion expresses the frequency separation requirements. A reduced-order version of the LPV/H_∞ controller is also proposed to handle an embedded implementation with limited computational burden. The nonlinear multi-source system is simulated in MATLAB® /Simulink® using two different types of driving cycles: the driving cycle of IFSTTAR (Institut Français des Sciences et Technologies des Transports, de l'Aménagement et des Réseaux) and a constant load profile used in order to illustrate system steady-state behaviour. Simulation results show good performance in supplying the load at constant DC-link voltage according to user-configured frequency-separation power sharing strategy. When assessed against the classical-PI-based filtering strategy taken as base-line, the proposed strategy offers the possibility of integrating a variety of constraints into a systematic design procedure, whose result guarantees stability and performance robustness.

Keywords: H_∞ control, LPV systems, power source coordination, reduced-order controller, frequency separation, electric vehicle.

1 INTRODUCTION

Global warming and increased need of petroleum products are main issues nowadays. Lots of research works focus on decreasing CO_2 emission by developing hybrid vehicles or electric ones equipped with a convenient solution that replaces combustion engines [1, 2]. Hybrid power supply systems use combination of fuel cell, battery and supercapacitor in order to satisfy power demand within electric vehicles. However, fuel cell could be combined with battery and supercapacitor in order to achieve power and energy density values similar to an ordinary engine [3], and it is expected that fuel cell/battery/supercapacitor hybrid could result in improved system performances and energy efficiency [4].

Fuel cell is a promising energy system for sustainable future due to its environment friendliness and modularity. The main drawback of a fuel cell power generation system is its slow dynamics because the fuel cell current slope must be limited to prevent fuel starvation and to improve its performance and lifetime. Besides, high cost per power unit and inability to allow bi-directional power flow are some drawbacks [5, 6]. Batteries also enable an important pollutant emission reduction and fuel consumption, but have some drawbacks such as low power density in comparison with supercapacitors (long charging time), low energy density in comparison with fuel cell (limited range), a high cost per power unit and a shorter lifetime [7]. According to Ragone's plot [8], sources can be classified into two main classes: high-energy-density sources that can supply power for long duration of time (*e.g.*, fuel cells), and high-power-density sources, which can provide relatively high power for short period of time (*e.g.*, supercapacitors). Batteries are classified in between the two classes depending on the battery type.

In order to achieve hybridization between the three power sources (fuel cell is main power source, battery and supercapacitor are auxiliary power sources), many configuration topologies are proposed regarding the number of components, energy management complexity and performance reliability. There are three main topological architectures: series, parallel, and cascaded [9, 10, 11]. In this paper, the parallel structure is chosen due to its flexibility to adapt the system parameters such that DC-bus value, sources' independence, and even the facility to replace or to add more power sources (photovoltaic panels, grid electricity, *etc...*).

In the literature, many works are dedicated to design high-performance and efficient energy management systems for a variety of application with two or three different power sources. A significant number of strategies can be found such as switching strategy [12], equivalent consumption minimization strategy [13], proportional-integral controllers [14], fuzzy logic control [15, 16], filtering strategy [17, 18, 19], sliding mode control [20], and LQG optimal control [21].

This paper deals with on-board energy management for a three-power-source power supply system (fuel cell, battery and supercapacitor) used in a parallel structure, where each source is controlled by means of a DC-DC converter. The sources

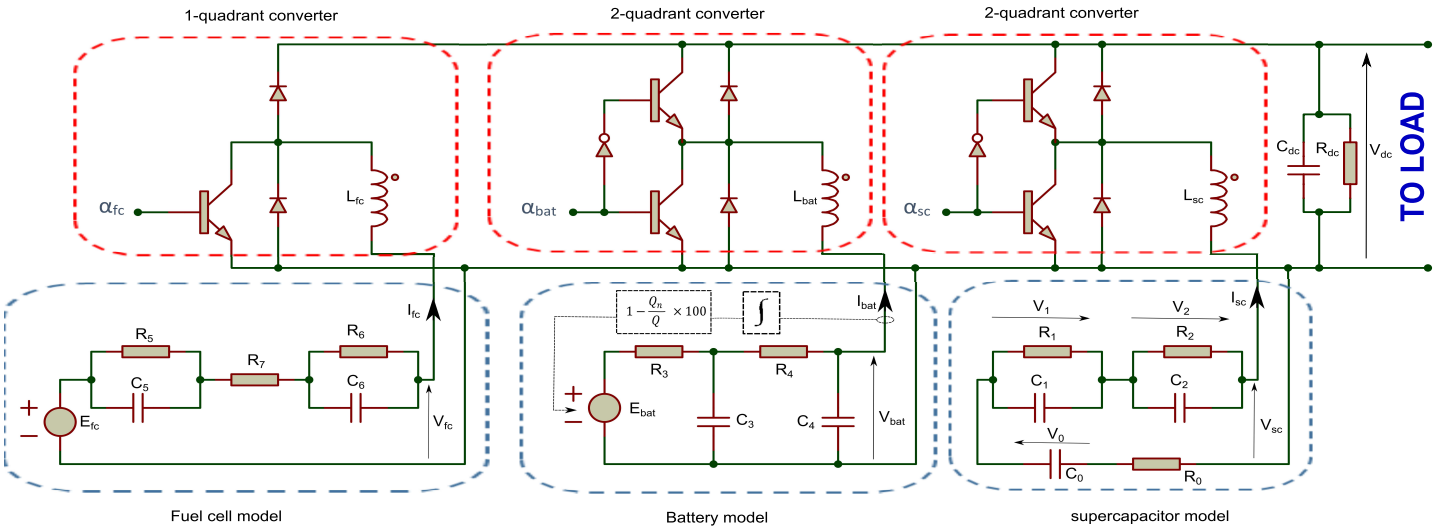

Figure 1: Considered system structure.

are connected in parallel to the load (consisting of an electrical motor with its associated converter) through a DC-bus (Fig.1). The main power source is the fuel cell connected to a 1-quadrant boost converter, whereas auxiliary sources are the battery and the supercapacitor; their role is to respond to power demand variations placed in relatively high frequency and to collect the reversed power (during braking phase). Each auxiliary source is connected to a 2-quadrant converter which allows charging/discharging. The sources are coordinated in a manner related to the frequency characterization of each one, which protects fuel cell and battery from high variation in power demand and in consequence prolong their lifetimes. The proposed strategy is formulated in the LPV/H_∞ framework methodology which leads to robust stability of the closed-loop behaviour.

This paper extends the authors' work in [22] by using a reduced-order version of the LPV/H_∞ controller, which is compared with the original one. Moreover, the control system is tested here using the driving cycle of IFSTTAR (Institut Français des Sciences et Technologies des Transports, de l'Aménagement et des Réseaux) that represents suburban driving features. This cycle has been preferred here because it has richer frequency content than, for example, the Normalized European Driving Cycle (NEDC), and, thus, it is more illustrative for the frequency separation validation. Steady-state source's behaviours are also examined.

The paper main contributions can be summarized in the following points:

- This paper proposes a generic solution that can be used as energy management system for power supply systems with potentially any number of power sources.
- The solution can handle the variations in system parameters due to LPV approach used in modeling and control design.
- An original frequency separation technique is proposed based on the choice of weighting functions associated to $\mathcal{H}_\infty$ control design. This can be applied to solve several power sources coordination problems.
- From application point of view, MORE toolbox [23] can be used to perform order-reduction for the LPV controller within specified frequency intervals. It is the method of LPV controller order reduction that is used here in order to reduce the computational burden when it is about practical implementation.
- The use of $\mathcal{H}_\infty$ control design allows to handle the load power demand without any prediction or estimation of its behavior. However, load current can be measured to modify the setpoint of the fuel cell and the battery steady-state behaviors.
- Detailed nonlinear models of the different parts of the studied system are used for simulation purpose in order to achieve and study the closed-loop behavior under as realistic as possible conditions.

This paper is organized as follows: Section 2 details power sources, converters and DC-bus models. The control problem is formulated in Section 3. The proposed solution is presented in Section 4, along with a method to reduce the controller order. Section 5 details the simulation results, including a comparison with a classical-PI-based filtering strategy taken as base-line. Section 6 concludes the paper.

2 MODELLING

This section is dedicated to present the system model starting from ordinary differential equations that represent physical laws. In general, vehicle's power supply system may be divided into three stages:

- Input stage: this stage represents the power sources in the vehicle. The main power source is assumed to be the fuel cell, whereas the auxiliary ones are the battery and the supercapacitor. Fig.1 shows the electrical models of the three power sources.

  The dynamics of the fuel cell and the battery are not considered in the LPV/H_∞ control problem. However more detailed models will be used for simulation purposes [24, 25].

  The supercapacitor state of charge is chosen to be controlled to handle the response to load variations during acceleration/braking phases. Supercapacitor electrical model shown in Fig.1 leads to following equations [26]:

$$\begin{cases} \frac{dV_0}{dt} = & \frac{-1}{C_0} I_{sc} \\ \frac{dV_1}{dt} = & \frac{-1}{C_1 R_1} V_1 - \frac{1}{C_1} I_{sc} \\ \frac{dV_2}{dt} = & \frac{-1}{C_2 R_2} V_2 - \frac{1}{C_2} I_{sc} \\ V_{sc} = & -I_{sc} R_0 + V_0 + V_1 + V_2 \end{cases} \tag{1}$$

  where I_{sc} is the supercapacitor current, V_{sc} is supercapacitor voltage, R_0, C_0, R_1, C_1, R_2, and C_2 are constant parameters of supercapacitor model, V_0, V_1 and V_2 are sub-voltages represented in supercapacitor model (Fig.1).

- Output stage: usually called DC-bus, which supplies power to load (vehicle's DC or AC motor with its associated power converter whose model is out of scope of this paper). Without any loss of generality, the DC-bus dynamic is investigated by using an output capacitor, which leads to the following equation:

$$\frac{dV_{dc}}{dt} = \frac{1}{C_{dc}} [\frac{-1}{R_{dc}} V_{dc} - I_{Load} + I_{fc}(1 - \alpha_{fc}) + I_{bat}\alpha_{bat} + I_{sc}\alpha_{sc}] \tag{2}$$

  where I_{Load} is the load current, V_{dc} is the DC-bus voltage, C_{dc} and R_{dc} are the DC-bus capacitor and resistance, respectively.

- Conversion stage: it represents all converters used to adapt the inputs to the output. Each power source is attached to DC-DC power converter with respect to source type, *i.e.*, the fuel cell is connected to 1-quadrant which allows power flow in one direction, whereas battery and supercapacitor are connected to 2-quadrant converters that are able to charge/discharge the sources. All converters are connected in parallel to the output stage (load) Fig.1. Averaged models are considered [27], which leads to following equations:

$$\begin{cases} \frac{dI_{fc}}{dt} = \frac{1}{L_{fc}} [V_{fc} - R_{fc} I_{fc} - V_{dc}(1 - \alpha_{fc})] \\ \frac{dI_{sc}}{dt} = \frac{1}{L_{sc}} [V_{sc} - R_{sc} I_{sc} - V_{dc}\alpha_{sc}] \\ \frac{dI_{bat}}{dt} = \frac{1}{L_{bat}} [V_{bat} - R_{bat} I_{bat} - V_{dc}\alpha_{bat}] \end{cases} \tag{3}$$

  where I_{fc}, I_{bat}, and I_{sc} are the currents of fuel cell, battery, and supercapacitor sources, respectively. $\alpha_{fc}, \alpha_{bat}$, and α_{sc} are the corresponding converter averaged duty ratios (averaged pulse-width-modulation control signals). V_{fc} and V_{bat} are fuel cell and battery voltages, respectively. $L_{fc}, L_{bat}, L_{sc}, R_{fc}, R_{bat}$ and R_{sc} are the inductances and resistances of smoothing inductors for each power converter, respectively.

  This conversion stage is treated separately from the paper problem. To this end, low level current-control loops are used to handle the dynamics represented in (3), as explained in Section 3.2.

The system (1),(2) may be rewritten in LPV form as follows:

$$\begin{cases} \dot{x} = A \cdot x + B_1 \cdot w + B_2(\rho) \cdot u \\ y = C \cdot x + D \cdot u \end{cases} \tag{4}$$

where the state vector is $x = [V_{DC} \quad V_1 \quad V_2 \quad V_0]^T$, $w = I_{Load}$ is the load current which represents the disturbance input, $u = [I_{fc} \quad I_{bat} \quad I_{sc}]^T$ is the control input vector composed of fuel cell, battery and supercapacitor currents, respectively, and $\rho = [\rho_1 \quad \rho_2 \quad \rho_3]^T = [\alpha_{fc} \quad \alpha_{bat} \quad \alpha_{sc}]^T$ is the varying parameter vector. Matrices in (4) are:

$$A = \begin{bmatrix} \frac{-1}{C_{dc} R_{dc}} & 0 & 0 & 0 \\ 0 & \frac{-1}{C_1 R_1} & 0 & 0 \\ 0 & 0 & \frac{-1}{C_2 R_2} & 0 \\ 0 & 0 & 0 & 0 \end{bmatrix}$$

$$B_1 = \begin{bmatrix} \frac{-1}{C_{dc}} \\ 0 \\ 0 \\ 0 \end{bmatrix}, \qquad B_2 = \begin{bmatrix} \frac{1-\rho_1}{C_{dc}} & \frac{\rho_2}{C_{dc}} & \frac{\rho_3}{C_{dc}} \\ 0 & 0 & \frac{-1}{C_1} \\ 0 & 0 & \frac{-1}{C_2} \\ 0 & 0 & \frac{-1}{C_0} \end{bmatrix} \qquad C = \begin{bmatrix} 1 & 0 & 0 & 0 \\ 0 & 1 & 1 & 1 \end{bmatrix}, \qquad D = \begin{bmatrix} 0 & 0 & 0 \\ 0 & 0 & -R_0 \end{bmatrix}$$

In the considered approach each parameter ρ_i is assumed to be bounded by $[0.1, 0.9]$ (this corresponds to the averaged duty ratio accepted variation from 10% to 90%). Each parameter is supposed to be independent from the other parameters.

3 FORMULATION OF THE CONTROL PROBLEM

3.1 CONTROL OBJECTIVES

This section summarizes the main goals of the proposed energy management system. Basically, some electrical constrains should be achieved with respect to power sources characteristics. The objectives are:

1. Keep the DC-bus voltage around $150V$ within an error of $\pm 10\%$ regardless of the load current variations.
2. Apply frequency separation to power sources, *i.e.*, each power source supplies power with respect to its characteristic frequency according to Ragone's classification [8]. This helps to protect the fuel cell and battery from harmful fast changes of load current. Frequency separation is achieved due to some suitable choice of weighting functions associated to H_∞ control design.
3. Maintain the supercapacitor state of charge (SOC) slowly around 50%, which allows to absorb/provide power to fulfil instantaneous load power demand.
4. Impose a desired steady-state behaviour for the rest of the power sources (fuel cell and battery) that corresponds to some desired power sharing between sources in steady state. This allows to operate the fuel cell at desired working point, *e.g.*, which corresponds to maximum efficiency. Steady-state behaviour could be used to determine battery charging cycle for long term with respect to its type. Battery charging could be achieved by using the main power source (fuel cell).

The hierarchical control strategy proposed in this paper consists of two loops: the current control loops on a lower level, and the energy management strategy corresponding to the LPV/H_∞ control loop shown in Fig.2.a. This latter loop provides references for the lower-level loop.

For sake of comparison, the block diagram of an energy management system using a PI-based filtering strategy is given in Fig.2.b. It consists of a cascade structure where the DC-link voltage regulation controller provides total current reference, whose components obtained by appropriate filtering are sent as references for the sources' current control loops. The filters' types and their cut-off frequencies are chosen in an empirical way depending on the desired dynamic behaviour of the associated power source in regulating the DC-bus voltage. For each power source, the desired behaviour is related to reliability and exploitation constraints recommended by the manufacturer. Therefore in this application, the fuel cell current reference is obtained by using a low-pass filter, which leads to slow variation of fuel cell current, while the battery current is filtered by using a bandpass filter, and finally the supercapacitor current is filtered using a high-pass filter, thus corresponding to supercapacitor ability in providing a fast-variable contribution to DC-bus regulation.. A supercapacitor SOC controller is also present, which provides a low-frequency component current reference to the supercapacitor, thus allowing to keep the SOC slowly around a desired setpoint (50%).

Performances of the two strategies will be comparatively assessed by numerical simulation in Section 5.

3.2 CURRENT CONTROL LOOPS (LOWER-LEVEL CONTROL)

Each power source current must be controlled and prevented from exceeding admissible limits. Therefore, three classical PI controllers are used to control the converters' dynamics represented in (3). These classical loops are designed [28] to be transparent to the outer level (have faster dynamics), and to satisfy tracking of all current references generated by LPV/H_∞ controller placed on the upper level (Fig.2.a). These current references are fuel cell current reference ${I_{fc}}^*$, battery current reference ${I_{bat}}^*$, and supercapacitor current reference ${I_{sc}}^*$. As consequence, we will consider in the sequel ${I_{fc}}^*=I_{fc}$, ${I_{bat}}^*=I_{bat}$ and ${I_{sc}}^*=I_{sc}$.

3.3 LPV/H_∞ CONTROL DESIGN (UPPER-LEVEL CONTROL)

The LPV controller $K(\rho)$ in Fig.2.a should satisfy the performance requirements given in Section 3.1. The controller design is tackled in the H_∞ framework applied to LPV systems. The control design scheme is given in Fig.3, where usual forms of the weighting functions are considered to represent the performance objectives, as explained below:

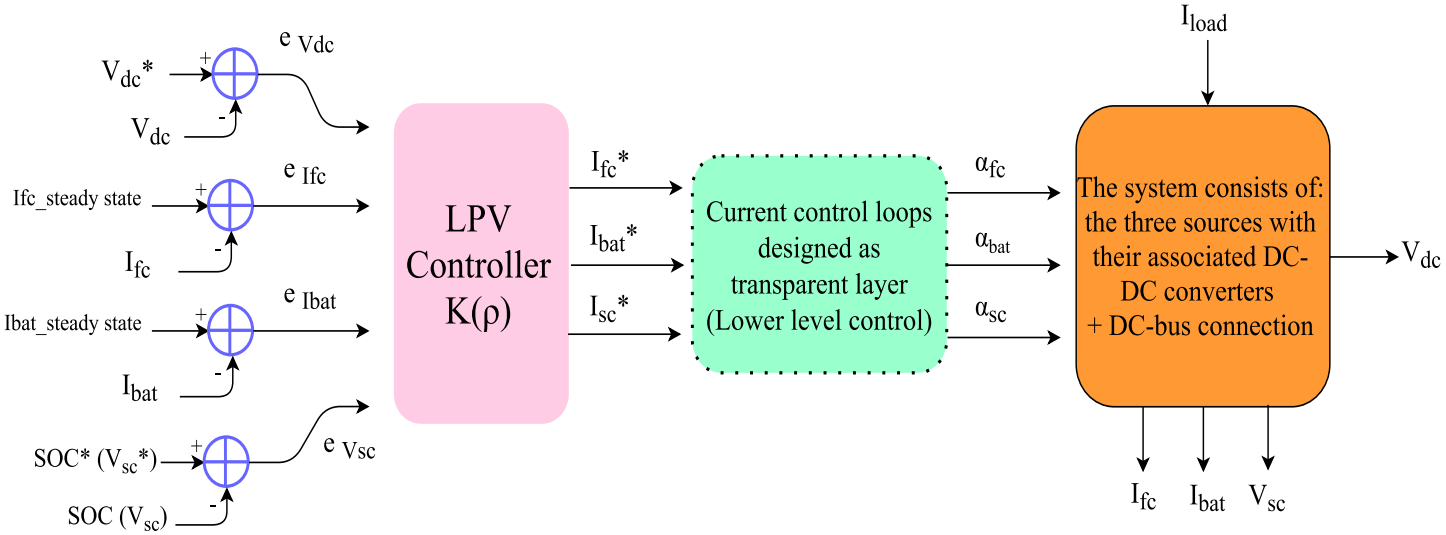

(a) Global control block diagram using LPV strategy.

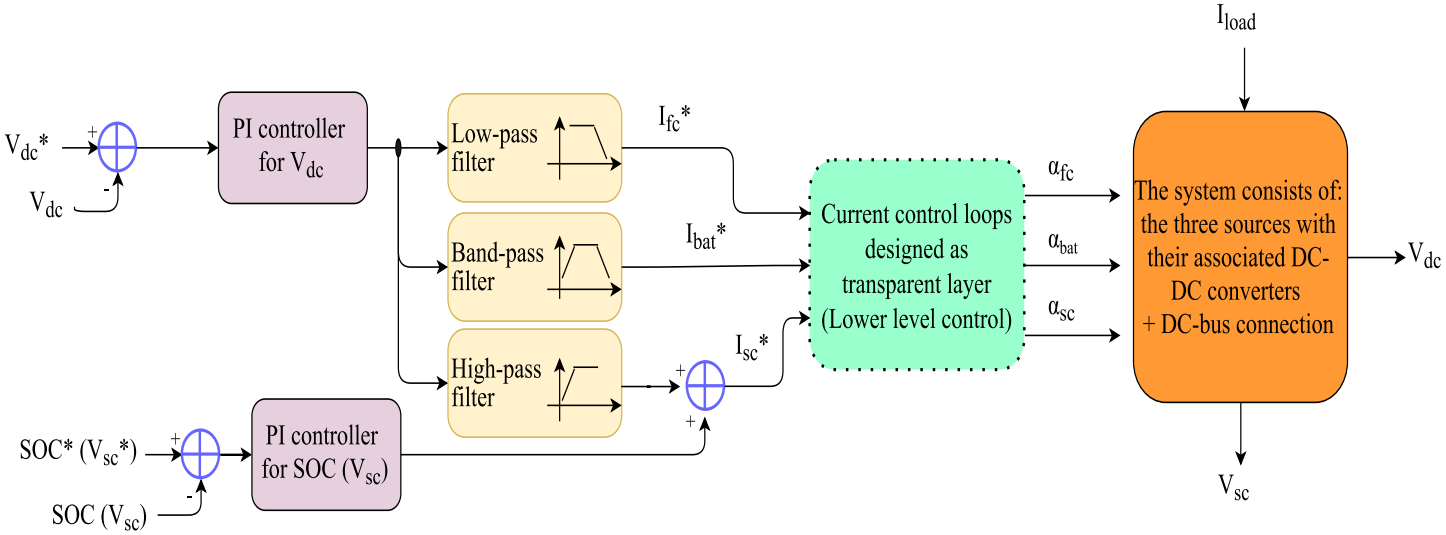

(b) Control block diagram using a classical-PI-based filtering strategy.

Figure 2: Different control strategies used to implement the energy management system: (a) the proposed LPV control diagram, (b) a classical-PI-based filtering strategy used for comparison.

1. DC-bus voltage (V_{DC}) tracking: $W_{eV_{dc}}$ is in charge to ensure both desired time response and acceptable tracking error range. To this end, a first-order weighting function is used.

2. Supercapacitor state of charge (SOC) regulation: a first-order function $W_{eV_{sc}}$ is used to maintain supercapacitor state of charge (SOC) around 50%. Consequently, the supercapacitor's SOC is a direct image of its voltage V_{sc} and can be calculated by using the following equation:

$$SOC = \frac{V_{sc} - V_{sc,min}}{V_{sc,max} - V_{sc,min}} \times 100\%, \tag{5}$$

   where $V_{sc,max}$ is the maximum allowed supercapacitor's voltage corresponding to SOC=100% and $V_{sc,min}$ is the minimum allowed supercapacitor's voltage corresponding to SOC=0%. Note that $V_{sc,min}$ must be different from zero and it is decided regarding the minimum allowed voltage input for the supercapacitor DC-DC converter.

3. Power sources separation with respect to their characteristic frequencies: W_{uIfc}, W_{uIbat} and W_{uIsc} shape the dynamic behaviour of current references of the fuel cell, the battery and the supercapacitor, respectively, according to some pre-specified frequency ranges. Both W_{uIbat} and W_{uIsc} are chosen as fourth-order transfer functions in order to achieve better dynamic separation within narrow frequency range, while W_{uIfc} is used in form of a first-order function.

4. Fuel cell and battery steady-state behaviours: $W_{eI_{fc}}$ and $W_{eI_{bat}}$ are used as constant values to determine fuel cell and battery long-term behaviours, respectively. In this way a desired steady-state power sharing can be imposed by using $I_{fc_{steadystate}}$ and $I_{batsteadystate}$ exogenous inputs.

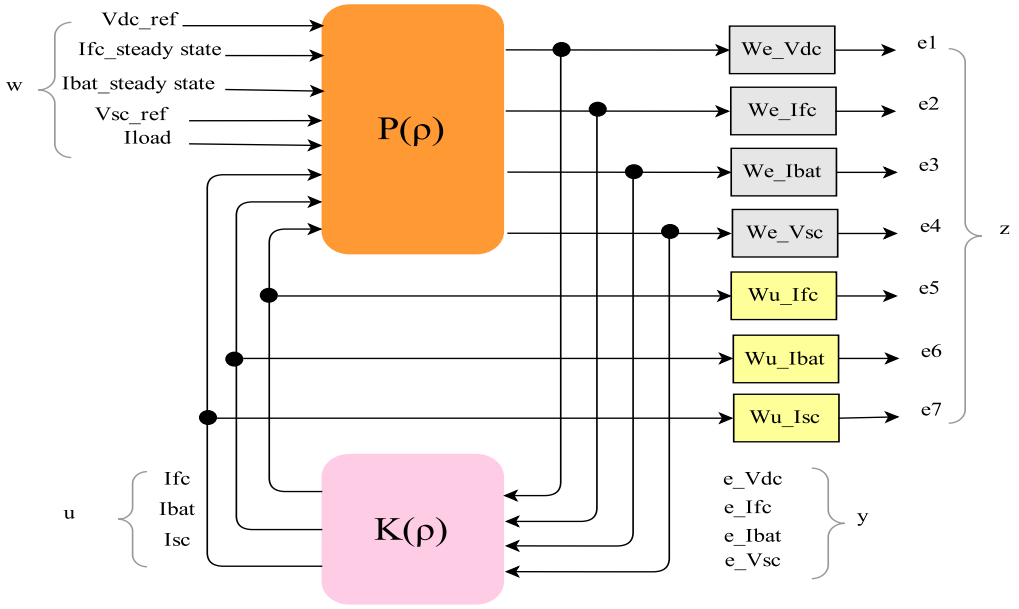

Figure 3: H_∞ Robust control design block diagram.

According to Fig.3, the considered control problem is to find an LPV controller $K(\rho)$ that ensures the closed-loop stability for all parameter variations and satisfies $\frac{\|e\|_2}{\|w\|_2} < \gamma_\infty$, where w is the exogenous input vector $w = [V_{dc_{ref}}, I_{fc_{steadystate}}, I_{bat\,steadystate}, V_{sc_{ref}}, I_{load}]$, and e is the controlled output vector $e = [e_1, e_2, ..., e_7]$.

4 CONTROL DESIGN SOLUTION

In order to obtain a controller that meets the control objectives, a set of Linear Matrix Inequalities (LMI) is solved [29] in the context of LPV/H_∞ control synthesis. The choice of weighting functions (associated to H_∞ control problem) is essential to meet frequency separation according to sources' characteristics. This is not a trivial process since there exist 19 parameters to be determined. Different approaches can be used in order to find a suitable parameter set such that heuristic methods, neural networks or some evolutionary algorithm. One of the most known class of evolutionary algorithms is genetic algorithms, which can be used to facilitate the weighting functions parameter choice in an automatic way. Because convergence to optimality is guaranteed, progress of iterations can be stopped when the solution is considered sufficiently good in relation to the predefined objective functions. An arbitrary stop criterion like maximum number of iterations may thus be used. Fig.4.a shows the steps followed to find the LPV/H_∞ controller.

4.1 LPV/H_∞ CONTROLLER

System in (4) can be rewritten under a polytopic form with $2^3 = 8$ vertices (since the parameter vector ρ has three bounded elements between [0.1,0.9]). The generalized LPV MIMO system is represented as following:

$$\begin{bmatrix} \dot{x} \\ z \\ y \end{bmatrix} = \begin{bmatrix} A & B_1 & B_2(\rho) \\ C_1 & D_{11} & D_{12} \\ C_2 & D_{21} & D_{22} \end{bmatrix} \begin{bmatrix} x \\ w \\ u \end{bmatrix} \tag{6}$$

The polytopic approach [29] is used to find the desired LPV/H_∞ controller. According to the methodology in the framework of quadratic stabilization described in [30, 31], the problem is treated off line by solving a set of LMIs using Yalmip/Sedumi solver (convex optimisation using single Lyapunov function, *i.e.*, quadratic stabilization) at each vertices of the polytope, which leads to vertex controllers $K_i = \begin{bmatrix} A_i & B_i \\ C_i & D_i \end{bmatrix}$ with $1 \leq i \leq 8$. The LPV controller $K(\rho)$ is computed on line as a convex combination of the vertices controllers K_i as follows:

$$K(\rho) = \sum_{1}^{8} \alpha_i(\rho) K_i \tag{7}$$

with:

$$\alpha_i(\rho) = \frac{\prod_{j=1}^{3} |\rho_j - C(w_i)_j)|}{\prod_{j=1}^{3} \left|\overline{\rho_j} - \underline{\rho_j})\right|} > 0, \quad \sum_{1}^{8} \alpha_i = 1$$

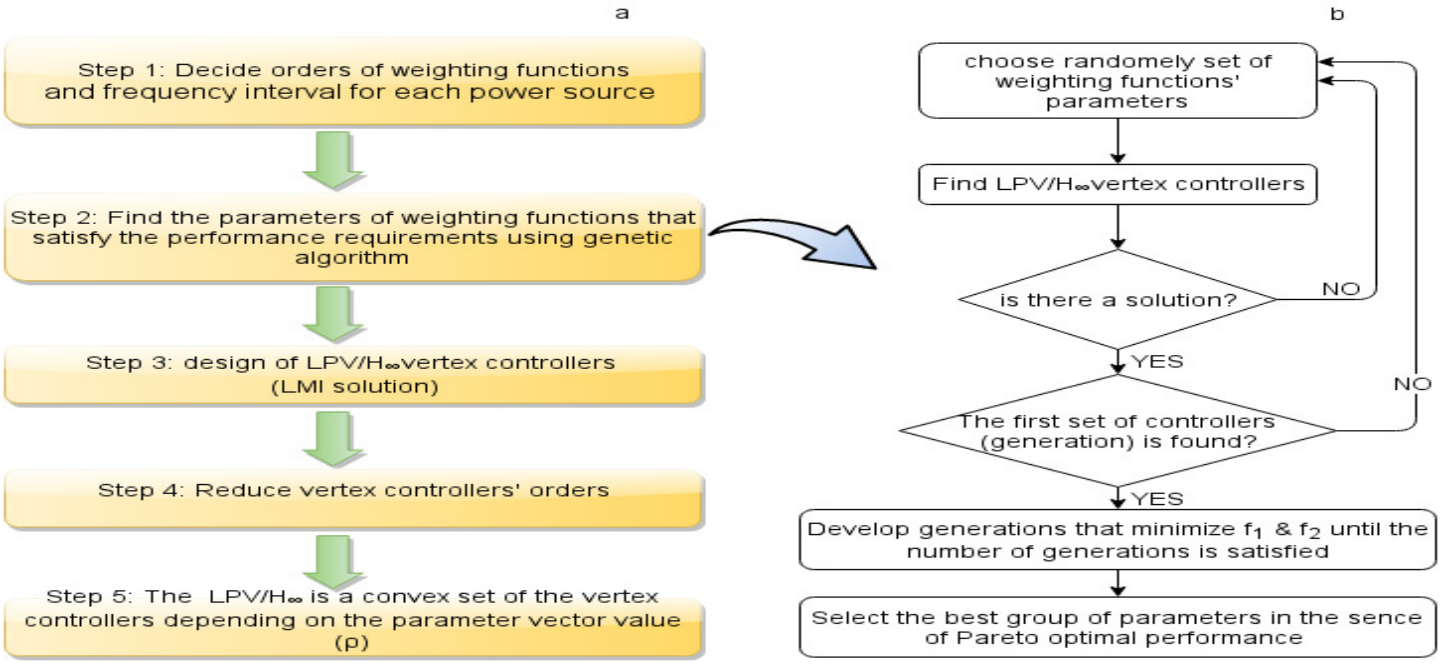

Figure 4: LPV/H_∞ controller design procedure.

where w_i are the vertices of the polytope corresponding to the extreme values of the parameter vector ρ. $C(w_i)_j$ is the j^{th} component of the vector $C(w_i)$ defined as:

$$C(w_i)_j = \begin{cases} \overline{\rho_j} & if \quad w_i = \underline{\rho_j} \\ \underline{\rho_j} & otherwise \end{cases}$$

where in this application

$$\overline{\rho_j} = max(\rho_j) = 0.9, \qquad \underline{\rho_j} = min(\rho_j) = 0.1$$

4.2 SELECTION OF WEIGHTING FUNCTIONS USING GENETIC ALGORITHMS

Genetic algorithms (GA) are used to find weighting functions' parameters used in LPV/H_∞ synthesis. As shown in Fig.4.b, this method develops generations of parameters to satisfy desired criteria, where objective (cost) functions are required to be minimized in order to meet optimal performance [32, 33]. In our case, the genetic algorithm minimizes two objective functions:

- Objective function 1 (closed-loop stability): certain combinations of weighting functions' parameters lead to no solution during H_∞ control optimization, this is considered as unstable generation. On the contrary, if good parameters are found the solution is stable by the nature of optimality process, and this cost function allows to search for more stable solution in the sense that the real parts of closed-loop eigenvalues are smaller than a certain desired value δ. Objective function 1 is expressed as:

$$min\{f_1 = \max_i(Re(\lambda_i)) < -\delta : \delta > 0\} \tag{8}$$

  where $Re(\lambda_i)$ is the real part of the closed-loop eigenvalue λ_i.

- Objective function 2: this is used to ensure frequency splitting ability of weighting functions. It is based on minimizing the following criterion:

$$min\left\{f_2 = \frac{J_1 + J_2 + J_3}{3}\right\} \tag{9}$$

  with

$$J_1 = \frac{\left\|\frac{I_{fc}}{I_{load}}\right\|_{\infty,(\omega_1,\omega_2)}}{\left\|\frac{I_{fc}}{I_{load}}\right\|_{\infty}}$$

$$J_2 = \frac{1}{2}.\frac{\left\|\frac{I_{bat}}{I_{load}}\right\|_{\infty,(\omega_3,\omega_4)}}{\left\|\frac{I_{bat}}{I_{load}}\right\|_{\infty}} + \frac{1}{2}.\frac{\left\|\frac{I_{bat}}{I_{load}}\right\|_{\infty,(\omega_5,\omega_6)}}{\left\|\frac{I_{bat}}{I_{load}}\right\|_{\infty}}$$

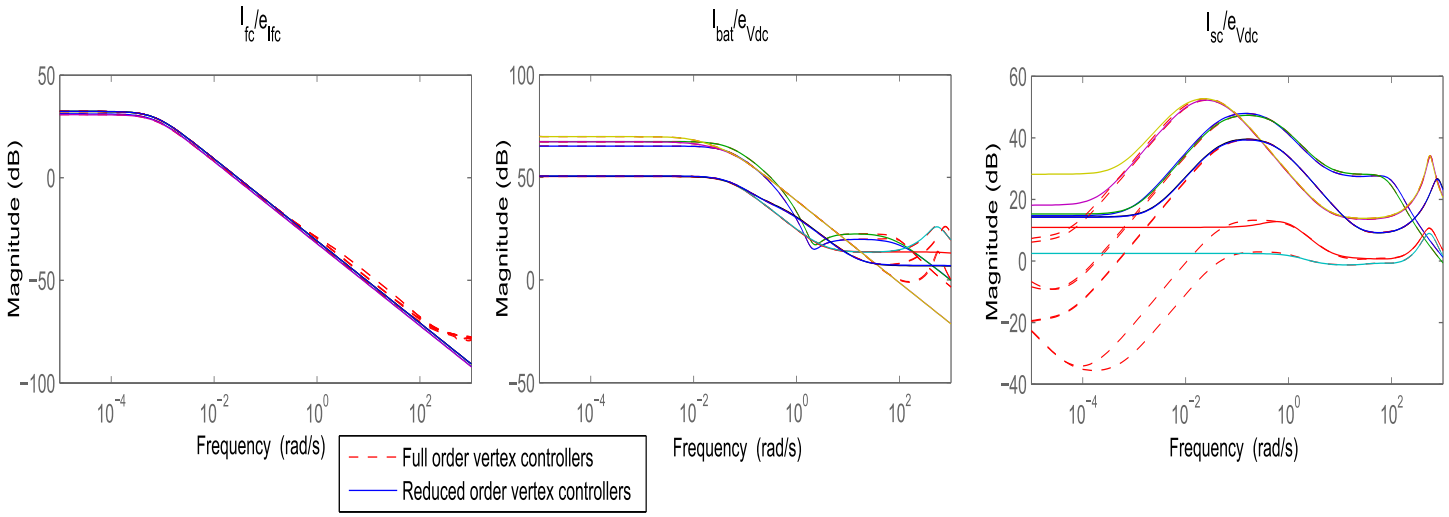

Figure 5: Frequency comparison between full-order and reduced-order vertex controllers.

$$J_3 = \frac{\left\| \frac{I_{sc}}{I_{load}} \right\|_{\infty,(\omega_7,\omega_8)}}{\left\| \frac{I_{sc}}{I_{load}} \right\|_{\infty}}$$

where $\|.\|_{\infty,(\omega_i,\omega_j)}$ is the H_∞ norm calculated within $[\omega_i, \omega_j]$ frequency interval. These criteria allow to minimize the H_∞-norm for each power source outside the desired working frequency interval of this source.

The criteria (8),(9) guarantees an arbitrary imposed degree of closed-loop stability and allow to size a desired frequency separation between power sources according to requirements of each application.

GA gives the following weighting functions used in LPV/H_∞ synthesis:

$$\begin{cases} \frac{1}{W_{eV_{dc}}} = \frac{s+\omega_b\cdot\epsilon}{s/M_s+\omega_b} = \frac{s+0.05}{0.5363s+500} \\ \frac{1}{W_{eI_{fc}}} = 3 \\ \frac{1}{W_{eI_{bat}}} = 1.9 \\ \frac{1}{W_{eV_{sc}}} = \frac{s+\omega_b\cdot\epsilon}{s/M_s+\omega_b} = \frac{s+0.0005}{0.5263s+0.05} \\ \frac{1}{W_{uI_{fc}}} = \frac{\epsilon\cdot s+\omega_{BC}}{s+\omega_{BC}/M_u} = \frac{0.9091s+0.07}{s+0.0007} \\ \frac{1}{W_{uI_{bat}}} = \left(\frac{\epsilon\cdot s+\omega_{BC}}{s+\omega_{BC}/M}\times\frac{s+\omega_b\cdot\epsilon}{s/M+\omega_b}\right)^2 = \frac{s^4+57.14s^3+816.3s^2+0.005714s+10^{-8}}{0.34s^4+0.01721s^3+2.858\times10^{-4}s^2+1.721\times10^{-6}s+3.4\times10^{-9}} \\ \frac{1}{W_{uI_{sc}}} = \left(\frac{\epsilon\cdot s+\omega_{BC}}{s+\omega_{BC}/M}\times\frac{s+\omega_b\cdot\epsilon}{s/M+\omega_b}\right)^2 = \frac{s^4+395s^3+3.907\times10^4s^2+1.185\times10^4s+900}{0.1413s^4+19.91s^3+709.5s^2+597.2s+127.2} \end{cases} \quad (10)$$

4.3 CONTROLLER ORDER REDUCTION

The full order LPV/H_∞ controller is a convex combination of eight controllers at the vertices of the polytope. Each of them is an LTI system with 18 states in its state-space representation. Model reduction is investigated in this work in order to reduce the complexity of the solution from practical implementation point of view. To this end, the MORE toolbox [23] is used to find a reduced-order model that fits the original controller for bounded frequency range. More precisely, Iterative SVD Tangential Krylov Algorithm (ISTIA) is applied on each vertex controller for a frequency range that contains all power sources characteristics, that is, for the whole bandwidth of the closed-loop system. The reduced-order vertex controllers are then found to be tenth-order dynamical systems.

The controller's transfer matrix contains 12 transfer functions that correspond to 4 inputs and 3 outputs (Fig.2.a). Fig.5 shows frequency fitness between original and reduced-order controller for some input/output transfer functions, whereas some other terms vanish due to reduction process (they have negligible values).

The performance of the full order LPV/H_∞ controller is compared with that of the reduced-order one. To this end, the considered criterion is the cost function in (9) and both H_∞, and H_2 norms of the closed-loop system. The comparison is done using the maximum obtained values among all vertices of the polytope and shown in Table 1.

Table 1: The cost function represented in (9) with $\mathcal{H}_2, \mathcal{H}_\infty$ Norms calculations for both reduced and full-order controllers.

	J_1	J_2	J_3	H_2	H_∞
Full-order controller O(18)	0.362	0.762	0.645	59.555	0.090
Reduced-order controller O(10)	0.371	0.794	0.624	59.082	1.099

One can notice that the values are close in view of the chosen criterion, even though the complexity is highly reduced.

5 SIMULATION

Numerical simulations are carried out using nonlinear electrical models for different system parts shown in Fig.1, where all dynamics of DC-DC converters, fuel cell and battery are taken into consideration (12 differential equations in total). The detailed models of different system parts have been validated on real-world data, being thus considered sufficiently accurate to represent the system behaviour in a numerical simulation context, as reported in previous works [19, 24]. IFSTTAR driving cycle [34] is chosen to prove the closed-loop system capability to cope with various driving modes and satisfy the required control objectives. This driving cycle is used next to represent the load demands in supporting a numerical-simulation comparison between the obtained reduced-order LPV controller and a base-line PI-based filtering strategy, as represented in Fig.2.b.

5.1 IFSTTAR TEST

The IFSTTAR profile represents various driving conditions, *i.e.*, acceleration, deceleration, fixed speed and full brake, which allow assessing performance of DC-bus voltage regulation and the way how the three sources are coordinated to satisfy the power demand. For this scenario, it is considered that load current is served exclusively by fuel cell in steady-state, hence no change demand for battery's SOC. For this reason, exogenous input references are fixed to $I_{fc_{steady-state}} = \frac{I_{load}}{1-\alpha_{fc}}$ and $I_{bat_{steady-state}} = 0$, respectively, where α_{fc} corresponds to the imposed steady state.

This load profile is rich in frequency content and challenges the vehicle's power supply management system in a way corresponding to urban driving conditions (Fig.6.a), where the DC-link current is an image of the vehicle speed. In the sequel, DC-link current is called load current for sake of simplicity.

The energy management system satisfy the control objectives as shown in Fig.6, where the DC-bus voltage is well regulated at voltage reference 150 V within accepted tracking error of $\pm 10\%$ (Fig.6.b). Power sources' currents are provided to the system in the manner of fuel cell supplying average current and supercapacitor handling peak variations, while the battery provides the midrange current variations as shown in Fig.6.d. In order to complete the analysis, the power spectral density of each source current is computed, then it is normalized with respect to the maximum power delivered by each source. According to Fig.8.a, each power source is used in distinct frequency zone according to the criteria choice J_1, J_2 and J_3 in genetic algorithm design (Section 4.2). Fuel cell is used in low-frequency range all the time, in contrast supercapacitor serves the relatively high-frequency load current variation, and finally battery is operated in between the other two sources. Another control objective is satisfied, where the supercapacitor state of charge is always kept within reasonable limits (avoiding extreme states, completely empty or completely full)(Fig.6.c).

For sake of comparison, the PI-based filtering strategy shown in Fig.2.b is also run in simulation. Note that it has a lot of parameters to be tuned manually; its cascade structure imposes in fact constraints on some of these parameters and prevents control objectives from being independently achieved. In particular, a relation between the imposed closed-loop bandwidth of the DC-link voltage regulation and filters' cut-off frequencies should *a priori* be set. Thus, a good combination of parameters for such strategy is difficult to be found while satisfying all control objectives. As clearly seen in Fig.6.b, the filtering strategy fails to regulate the DC-bus voltage within the accepted tracking error, whereas it has good performance regarding the frequency separation between power sources, according to Fig.8.b. Finally, there is no guarantee for the closed-loop stability. Different from this approach, the proposed LPV MIMO control strategy finds automatically the appropriate parameters of weighting functions using a genetic algorithm procedure that takes into account all control objectives (Section 3.1).

In a broader sense, the proposed strategy is a generalized filtering strategy in a MIMO context, *i.e.*, completed with certain degrees of freedom to meet a multitude of control goals, and optimized according to some user-defined criteria.

Important remark: The previous results are found using the reduced-order controller version (see Section 4.3). The original LPV/H_∞ controller leads to slightly better performance, but its practical implementation is more difficult because of its complexity.

Table 2 presents comparatively the values of the same optimization criteria as in Table 1, but this time for the reduced-order controller and for the filtering strategy, respectively. One can see that, manually parameter tuning without any systematic improvement or optimization approach makes the filtering strategy to performs worse.

Table 2: A comparison between the reduced-order controller and the filtering strategy (shown in Fig.2.b) with respect to the cost function represented in (9) with $\mathcal{H}_2, \mathcal{H}_\infty$ Norms calculations.

	J_1	J_2	J_3	H_2	H_∞
Reduced-order controller	0.371	0.794	0.624	59.082	1.099
Compared filtering strategy	0.740	0.818	0.801	66.474	7.201

5.2 STEADY-STATE TEST

Another simulation scenario is tested when the load has a step variation, in order to assess system steady-state behaviour. This scenario illustrates how the two proposed external inputs, $I_{fc_{steadystate}}$ and $I_{batsteadystate}$, determine the steady-state load sharing between fuel cell and battery. Negative battery current value can be used in order to charge it in long term.

This test is used in order to illustrate the 4^{th} control objective (Section 3.1). A simple simulation scenario is given here, where the external reference inputs define steady-state distribution of the fuel cell and the battery currents. Therefore, a constant load current is applied which permits to reach steady-state equilibrium. Two different distributions are used to satisfy same constant load current (35 A):

- $I_{fc_{steadystate}} = \frac{0.70*35}{1-\alpha_{fc_{steadystate}}} = 81A$ and $I_{batsteadystate} = \frac{0.30*35}{\alpha_{batsteadystate}} = 30A$;
  this corresponds to $70\% I_{load}$ supplied by the fuel cell and 30% by the battery (Fig.8.a).
- $I_{fc_{steadystate}} = \frac{1.30*35}{1-\alpha_{fc_{steadystate}}} = 190A$ and $I_{batsteadystate} = \frac{-0.30*35}{\alpha_{batsteadystate}} = -24.5A$;
  this corresponds to 130% I_{load} supplied by the fuel cell and -30% by the battery, meaning that the fuel cell is managed to supply load current and to charge the battery in the same time (Fig.8.b).

Fig.8 shows the slowly varying I_{fc} and I_{bat} currents corresponding to the constant load. From an application point of view, these two external inputs are useful to impose a desired steady-state operating point. Note that there exists a slight tracking error which could be reduced by using more complex weighting functions $W_{eI_{fc}}$ and $W_{eI_{bat}}$.

6 CONCLUSION

In this paper, an energy management strategy based on multi-variable LPV/H_∞ control is presented. This approach allows to coordinate power sources of different types within off-grid applications. The studied system is based on three different kinds of power sources – fuel cell, battery and supercapacitor – on board of an electric vehicle. Current-controlled sources are connected in parallel with their associated DC-DC boost converters on a common DC-bus. The DC-bus voltage is regulated in spite of load power variations that represent the image of driving cycle. Fuel cell and battery are protected from sudden power variations in order to prolong their lives. Thus, each source is operated in the frequency range which best suits its characteristics as either high-energy-density or high-power-density source, according to Ragone's taxonomy. Therefore, fuel cell is managed to provide low-frequency current (mean power), supercapacitor provides/absorbs sudden variations in power demand, while battery operation is placed in between the other two sources. Frequency-separation requirements are cast into an optimization criterion used to guide computation of H_∞ weighting functions by means of a genetic algorithm. The LPV/H_∞ controller based on the polytopic approach guarantees the quadratic-stability of the closed-loop system for all parameter variations. A reduced-order version of the full-order controller is also presented, which is a valuable step to reduce complexity from a practical implementation point of view.

The parallel configuration and use of MIMO control strategy allow to generalize this concept to any system equipped with potentially any number of power sources. The proposed strategy is generic and results in a systematic way while guaranteeing stability and robustness performance for the entire operating range. The possibility of imposing a desired steady-state behaviour is another advantage. For example, fuel cell operation at the maximum-efficiency point may be allowed in this way, thus increasing the total system autonomy. Applying frequency separation protects the fuel cell and the battery from sudden variation in current demand; therefore these sources are operated in better conditions and this helps to prolong their lifetimes. Ageing models must be considered in future study to quantitatively assess the advantage of frequency separation on power source lifetime.

Nonlinear electrical system is simulated using the IFSTTAR standardized driving profile, whose frequency content is rich and allows to properly illustrate the frequency separation ability of the proposed approach. Numerical simulation results show good performance in meeting the vehicle's power demand according to the frequency-separation power sharing regime imposed by user, all by regulating the DC-bus voltage at a desired setpoint.

This work can be extended to smart-grid applications, wherever different technologies are used to supply and/or store energy. Therefore, generalization of the proposed power sharing control strategy within multi-source application potentially containing any number of power sources, can easily be envisaged. An experimental validation on a dedicated test bench is in progress in collaboration with Systèmes Et Transports (SET) Laboratory in Belfort, France.

7 Appendix

Table 3: Electrical system parameters used for simulation results.

Parameter	description	simulation value
DC-bus		
V_{DC}	DC-bus voltage	150 V
C_{DC}	DC-bus capacitor	2.0×10^{-3} F
R_{DC}	DC-bus discharging resistor	$10.0 \times 10^{+3}$ Ω
Fuel cell		
L_{fc}	Fuel cell converter's inductor	2.0×10^{-3} H
E_0	Fuel cell open-circuit voltage	50 V
R_m	Fuel cell model's resistor	7.63×10^{-2} Ω
R_{ta}	Fuel cell model's resistor	2.0×10^{-3} Ω
R_{tc}	Fuel cell model's resistor	4.72×10^{-4} Ω
C_a	Fuel cell model's capacitor	2.12×10^{-3} F
C_c	Fuel cell model's capacitor	2.12×10^{-2} F
Battery		
L_{bat}	Battery converter's inductor	1.0×10^{-3} H
Q_n	Initial SOC of battery	70 %
C_1	Battery model's capacitor	2.92×10^{-4} F
R_1	Battery model's resistor	13.4×10^{-3} Ω
C_2	Battery model's capacitor	2.92×10^{-4} F
R_2	Battery model's resistor	13.4×10^{-3} Ω
Nominal V_{bat}	The nominal battery's voltage	48 V
Supercapacitor		
L_{sc}	Supercapacitor converter's inductor	1.0×10^{-3} H
R_s	Supercapacitor model's resistor	0.8×10^{-3} Ω
C_0	Supercapacitor model's capacitor	56.0 F
C_1	Supercapacitor model's capacitor	1.0 F
C_2	Supercapacitor model's capacitor	1.0 F
R_1	Supercapacitor model's resistor	6.0×10^{-4} Ω
R_2	Supercapacitor model's resistor	4.5×10^{-4} Ω
$V_{sc,max}$	Supercapacitor maximum voltage corresponds to SOC=100%	42 V
$V_{sc,min}$	Supercapacitor minimum voltage corresponds to SOC=0%	32 V
PIs local control loops		
Kp_{fc} , Ki_{fc}	PI parameters used for fuel cell current control loop	0.5 , 0.1
Kp_{bat} , Ki_{bat}	PI parameters used for battery current control loop	0.01 , 0.8
Kp_{sc} , Ki_{sc}	PI parameters used for supercapacitor current control loop	0.01 , 0.4

References

[1] J. Van Mierlo, G. Maggetto, and P. Lataire, "Which energy source for road transport in the future? a comparison of battery, hybrid and fuel cell vehicles," *Energy Conversion and Management*, vol. 47, pp. 2748–2760, Oct. 2006.

[2] P. Garcia, L. Fernandez, C. Garcia, and F. Jurado, "Fuel cell-battery hybrid system for transport applications," in *International Conference on Electrical Machines and Systems, 2009. ICEMS 2009*, pp. 1–5, Nov. 2009.

[3] M. Hannan, F. Azidin, and A. Mohamed, "Analysis of multi-power sources energy management system for electric hybrid vehicle," in *2011 IEEE Ninth International Conference on Power Electronics and Drive Systems (PEDS)*, pp. 452–458, Dec. 2011.

[4] P. Thounthong, S. Raël, and B. Davat, "Energy management of fuel cell/battery/supercapacitor hybrid power source for vehicle applications," *Journal of Power Sources*, vol. 193, pp. 376–385, Aug. 2009.

[5] M. Nayeripour, M. Hoseintabar, and T. Niknam, "Frequency deviation control by coordination control of FC and double-layer capacitor in an autonomous hybrid renewable energy power generation system," *Renewable Energy*, vol. 36, pp. 1741–1746, June 2011.

[6] Z. Yu, D. Zinger, and A. Bose, "An innovative optimal power allocation strategy for fuel cell, battery and supercapacitor hybrid electric vehicle," *Journal of Power Sources*, vol. 196, pp. 2351–2359, Feb. 2011.

[7] A.-L. Allegre, A. Bouscayrol, and R. Trigui, "Flexible real-time control of a hybrid energy storage system for electric vehicles," *IET Electrical Systems in Transportation*, vol. 3, pp. 79–85, Sept. 2013.

[8] A. Kuperman and I. Aharon, "Battery/ultracapacitor hybrids for pulsed current loads: A review," *Renewable and Sustainable Energy Reviews*, vol. 15, pp. 981–992, Feb. 2011.

[9] T. Azib, C. Larouci, A. Chaibet, and M. Boukhnifer, "Online energy management strategy of a hybrid fuel cell/battery/ultracapacitor vehicular power system," *IEEJ Transactions on Electrical and Electronic Engineering*, vol. 9, pp. 548–554, Sept. 2014.

[10] S. F. Tie and C. W. Tan, "A review of energy sources and energy management system in electric vehicles," *Renewable and Sustainable Energy Reviews*, vol. 20, pp. 82–102, Apr. 2013.

[11] I. Aharon and A. Kuperman, "Topological overview of powertrains for battery-powered vehicles with range extenders," *IEEE Transactions on Power Electronics*, vol. 26, pp. 868–876, Mar. 2011.

[12] M. Hannan, F. Azidin, A. Mohamed, and M. Uddin, "Test bench model and algorithms for multi-sources light electric vehicle energy management system," in *Industry Applications Society Annual Meeting, 2015 IEEE*, pp. 1–8, Oct 2015.

[13] I. Aiteur, C. Vlad, and E. Godoy, "Energy management and control of a fuel cell/supercapacitor multi-source system for electric vehicles," in *System Theory, Control and Computing (ICSTCC), 2015 19th International Conference on*, pp. 797–802, Oct 2015.

[14] J. Wong, N. Idris, M. Anwari, and T. Taufik, "A parallel energy-sharing control for fuel cell-battery-ultracapacitor hybrid vehicle," in *2011 IEEE Energy Conversion Congress and Exposition (ECCE)*, pp. 2923–2929, Sept. 2011.

[15] O. Erdinc, B. Vural, and M. Uzunoglu, "A wavelet-fuzzy logic based energy management strategy for a fuel cell/battery/ultra-capacitor hybrid vehicular power system," *Journal of Power Sources*, vol. 194, pp. 369–380, Oct. 2009.

[16] A. Fadel and B. Zhou, "An experimental and analytical comparison study of power management methodologies of fuel cell, battery hybrid vehicles," *Journal of Power Sources*, vol. 196, pp. 3271–3279, Mar. 2011.

[17] M. Silva, J. Trovao, P. Pereirinha, and H. Jorge, "Application of a decoupling method based on online filtering technique for multi-source electric vehicles," in *2013 15th European Conference on Power Electronics and Applications (EPE)*, pp. 1–10, Sept. 2013.

[18] A. Florescu, S. Bacha, I. Munteanu, and A. Bratcu, "Frequency-separation-based energy management control strategy of power flows within electric vehicles using ultracapacitors," in *IECON 2012 - 38th Annual Conference on IEEE Industrial Electronics Society*, pp. 2957–2964, Oct. 2012.

[19] A. Florescu, S. Bacha, I. Munteanu, A. I. Bratcu, and A. Rumeau, "Adaptive frequency-separation-based energy management system for electric vehicles," *Journal of Power Sources*, vol. 280, pp. 410–421, Apr. 2015.

[20] J. Liu, S. Laghrouche, and M. Wack, "Observer-based higher order sliding mode control of power factor in three-phase ac/dc converter for hybrid electric vehicle applications," *International Journal of Control*, vol. 87, no. 6, pp. 1117–1130, 2014.

[21] A. Florescu, A. Bratcu, I. Munteanu, A. Rumeau, and S. Bacha, "LQG optimal control applied to on-board energy management system of all-electric vehicles," *IEEE Transactions on Control Systems Technology*, vol. 4, pp. 1427–1439, 2015.

[22] W. Nwesaty, A. I. Bratcu, and O. Sename, "Optimal frequency separation of power sources by multivariable lpv/h_∞ control: Application to on-board energy management systems of electric vehicles," in *IEEE 53rd Annual Conference on Decision and Control (CDC)*, pp. 5636–5641, Dec. 2014.

[23] C. Poussot-Vassal and P. Vuillemin, "Introduction to MORE: A MOdel REduction toolbox," in *2012 IEEE International Conference on Control Applications (CCA)*, pp. 776–781, Oct. 2012.

[24] D. Hernandez, D. Riu, O. Sename, and F. Druart, "A robust multivariable approach for hybrid fuel cell supercapacitor power generation system," *The European Physical Journal Applied Physics*, vol. 54, no. 02, 2011.

[25] M. Ceraolo, "New dynamical models of lead-acid batteries," *IEEE Transactions on Power Systems*, vol. 15, pp. 1184–1190, Nov. 2000.

[26] C. H. Wu, Y. H. Hung, and C. W. Hong, "On-line supercapacitor dynamic models for energy conversion and management," *Energy Conversion and Management*, vol. 53, pp. 337–345, Jan. 2012.

[27] S. Bacha, I. Munteanu, and A.I. Bratcu, *Power Electronics Converters Modelling and Control : With Case Studies*. London: Springer, "*A*dvanced *T*extbooks in *C*ontrol and *S*ignal *P*rocessing *S*eries" ed., 2013.

[28] Åström, K. J. and Högglund, T., *PID Controllers: Theory, Design, and Tuning*. Instrument Society of America, Research Triangle Park, NC, 2 ed., 1995.

[29] C. Scherer, P. Gahinet, and M. Chilali, "Multiobjective output-feedback control via LMI optimization," *IEEE Transactions on Automatic Control*, vol. 42, pp. 896–911, July 1997.

[30] P. Apkarian, P. Gahinet, and G. Becker, "Self-scheduled h_∞ control of linear parameter-varying systems: a design example," *Automatica*, vol. 31, pp. 1251–1261, Sept. 1995.

[31] A.-L. Do, O. Sename, and L. Dugard, "Lpv modeling and control of semi-active dampers in automotive systems," in *Control of Linear Parameter Varying Systems with Applications*, pp. 381–411, Springer, 2012.

[32] D. Goldberg and J. Holland, "Genetic algorithms and machine learning," *Machine Learning*, vol. 3, no. 2-3, pp. 95–99, 1988.

[33] E. Zitzler, M. Laumanns, and L. Thiele, *SPEA2: Improving the strength Pareto evolutionary algorithm*. Eidgenössische Technische Hochschule Zürich (ETH), Institut für Technische Informatik und Kommunikationsnetze (TIK), 2001.

[34] T. J. Barlow, S. Latham, I. McCrae, P. Boulter, and others, *A reference book of driving cycles for use in the measurement of road vehicle emissions*, vol. 1. 2009.

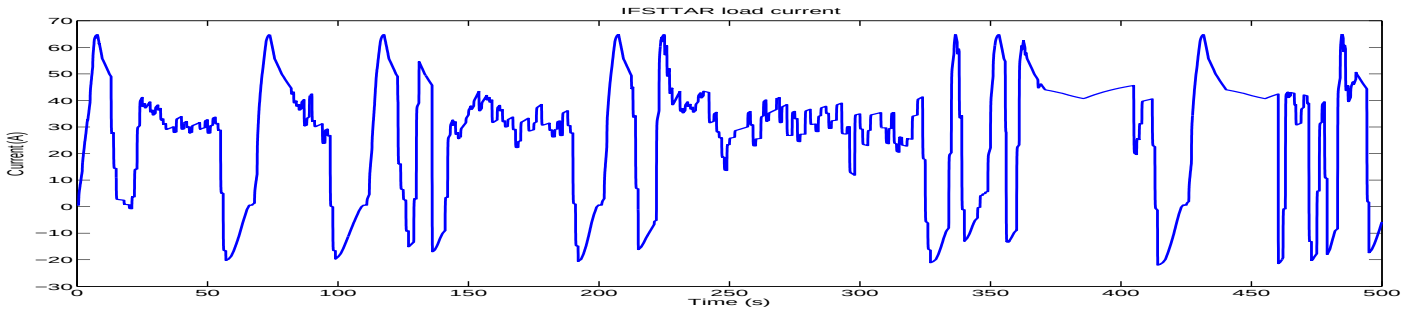

(a) IFSTTAR I_{load}

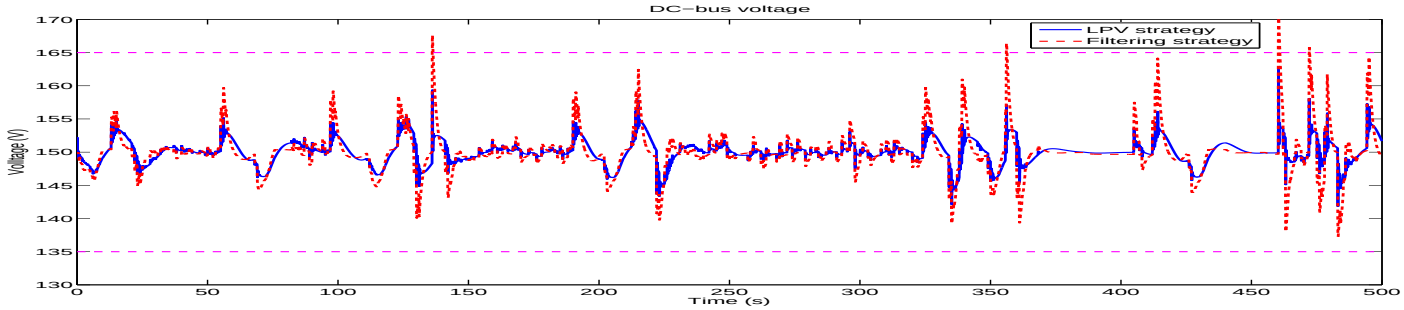

(b) DC-bus voltage corresponding to reduced-order LPV controller and ordinary filterring strategy

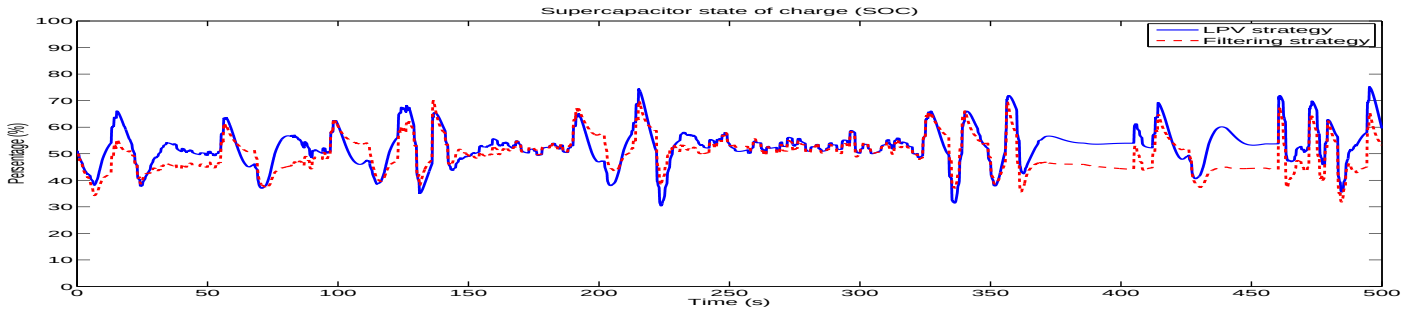

(c) Supercapacitor SOC corresponding to reduced-order LPV controller and ordinary filterring strategy

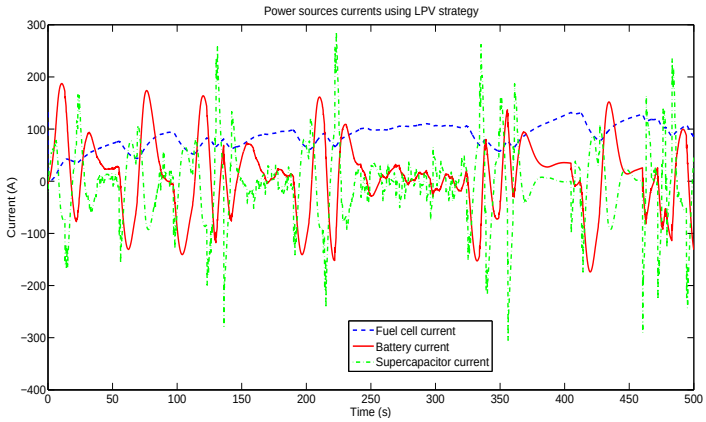

(d) Power sources' currents corresponding to reduced-order LPV controller

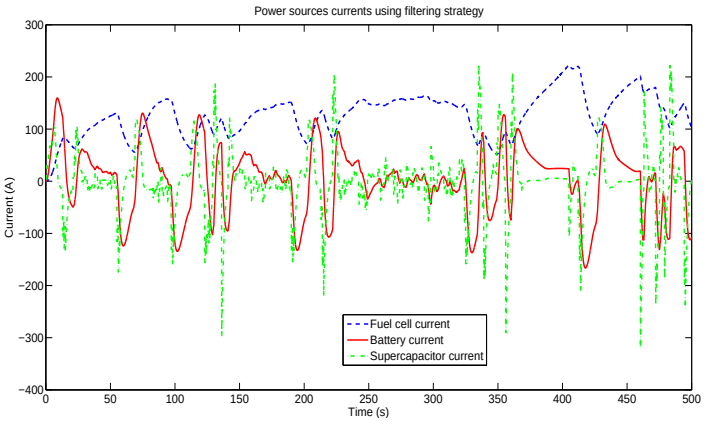

(e) Power sources' currennts corresponding to filtering strategy

Figure 6: Performance of the proposed reduced-order controller strategy compared to ordinary filtering strategy (shown in Fig.2.b) and corresponding to the IFSTTAR scenario.

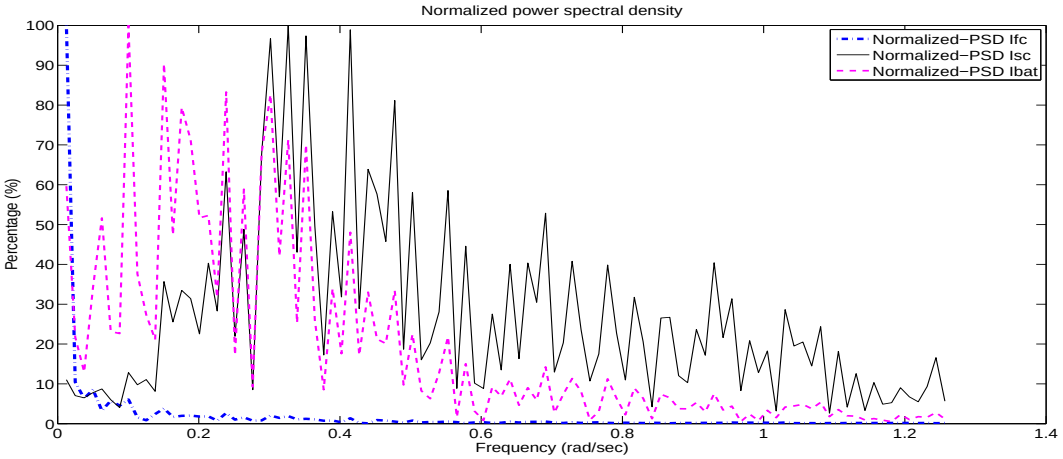

(a) Normalized power spectral density of sources' currents corresponding to reduced-order LPV strategy

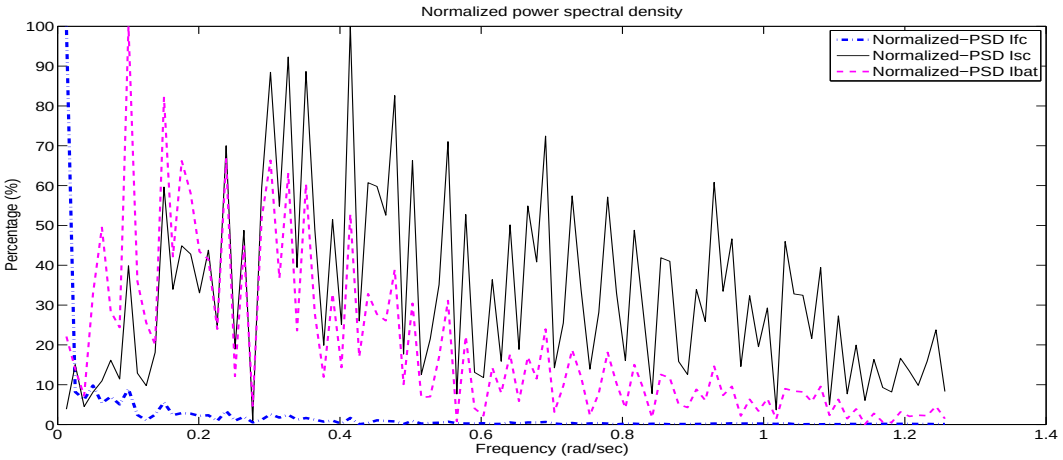

(b) Normalized power spectral density of sources' currents corresponding to filterring strategy

Figure 7: Frequency-domain spectral analysis corresponding to: a) proposed reduced-order LPV controller, b) filtering strategy (shown in Fig.2.b) and corresponding to the IFSTTAR scenario.

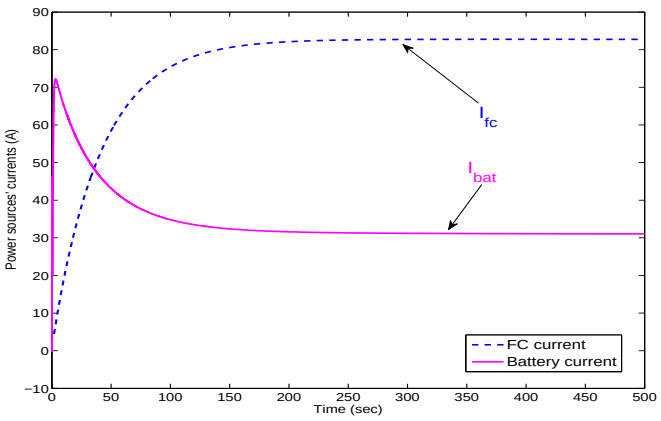

(a) Both fuel cell and battery have positive currents while satisfying the load demand and corresponding to the desired current reference setpoints.

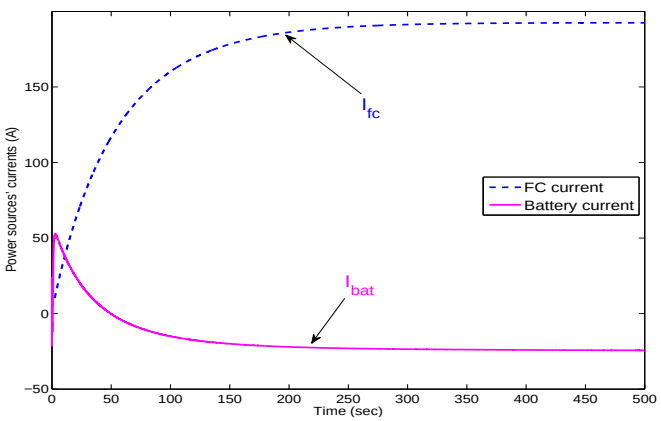

(b) Fuel cell has positive current while satisfying the load demand and charging the battery (negative current) corresponding to the desired current reference setpoints.

Figure 8: Steady-state scenarii for both fuel cell and battery (as described in Section 5.2) corresponding to a step of 35 A in load current demand.